Model-Predictive Spiral and Spin Upset Recovery Control for the Generic Transport Model Simulation*

Torbjørn Cunis,[1] Dominic Liao-McPherson,[1] Ilya Kolmanovsky,[1] and Laurent Burlion[2]

***Abstract*— Aircraft upsets are a major cause of fatalities in civil aviation. Unfortunately, recovery from upset scenarios is challenging due to the combination of nonlinearities, actuator limits, and upset modes. In this paper, we consider the use of Model-Predictive Control (MPC) in combination with a recently proposed piecewise polynomial prediction model, for six degree-of-freedom upset recovery. MPC naturally handles nonlinearities and constraints and has a provably large closed-loop region of attraction making it an appealing methodology for upset recovery problems. We present a recovery formulation then illustrate its utility through high fidelity simulation case studies, using the Generic Transport Model, of recovery from oscillatory spin and steep spiral upset conditions.**

I. Introduction

Over the past several decades, aircraft upset incidents have remained the "highest risk to civil aviation" [1]. As a result, upset recovery approaches have been extensively studied in the literature [2–5]. Proposed approaches include adaptive control [6], machine learning [7], and model-predictive control [8, 9] as well as state-machine based recovery strategies [10, 11]. Further approaches using recoverable sets have been developed and demonstrated in [12, 13].

The Generic Transport Model (GTM), developed by NASA and Boeing [14, 15], is an important benchmark for upset recovery methodologies. The GTMs upset dynamics have been extensively studied. In particular, Gill et al. [16] studied the upset dynamics of the GTM and identified dynamic regimes with rotary motion such as steep spirals, as well as oscillatory spins of period one and three, all of which are partially stable and attractive.

Model-Predictive Control (MPC) is an optimization based control methodology wherein a feedback law is defined as the solution of a receding horizon optimal control problem (OCP) parameterized by current measurements [17, 18]. MPC is well suited for the six degree-of-freedom (6dof) upset recovery problem, where the ailerons, elevator, and rudder must be coordinated while accounting for their physical limits, due to its ability to systematically handle nonlinearities and constraints. In this paper, we present an MPC scheme for six-degrees-of-freedom recovery and demonstrate its capabilities through spiral and spin upset recovery scenarios.

MPC relies on an appropriate prediction model to quantify the behaviour of the plant. However, a closed algebraic formulation of full-envelope aircraft dynamics is difficult to attain due to the complexity of post-stall aerodynamics [19]. In this paper, we use a recently proposed piecewise model of the GTM's aerodynamic coefficients [20] as (imperfect) prediction model and the GTM's high-fidelity simulation [21] as "real" system.

MPC has been well studied by the aeronautical community for general and fault-tolerant flight conditions [22, 23] but less so for upset recovery. For recovery of a piloted aircraft from a high-pitch upset, [8] generated guidance trajectories using linear-quadratic MPC. Moreover, in a previous paper [24], we discussed a loss-of-altitude minimizing economic MPC strategy for deep-stall recovery of a laterally pre-stabilized aircraft. To the best of our knowledge, spiral and spin recovery has only been addressed using ad-hoc, i.e., PID and heuristic-based, control techniques [25, 26].

This paper's main contribution is demonstrating that MPC offers a general and systematic methodology for designing upset recovery controllers. In addition, we demonstrate that the proposed piecewise polynomal model can sufficiently accurately predict the flight dynamics, both in normal flight and in the post-stall regime, to allow for successful closed-loop recoveries of the GTM.

Notation: Deflections of ailerons, elevator, and rudder are denoted by ξ, η, ζ, respectively, and are negative if leading to a positive moment. The aircraft's velocity vector with respect to air is written $\mathbf{V}_\mathrm{A}^\mathrm{T} = \begin{bmatrix} u & v & w \end{bmatrix}$ and it's body rates, $\boldsymbol{\omega}^\mathrm{T} = \begin{bmatrix} p & q & r \end{bmatrix}$; both are recorded in the ISO 1151-3 standard body axis system[27] with the x-axis along the fuselage, the y-axis to the right, and the z-axis oriented down to complete the orthogonal frame. The airspeed is denoted by $V_\mathrm{A} = \|\mathbf{V}_\mathrm{A}\|$ and the longitudinal and lateral relative wind angles, i.e., angle of attack and sideslip angle, are denoted by $\alpha = \arcsin\big(w/\sqrt{u^2+v^2}\big)$ and $\beta = \arcsin(v/V_\mathrm{A})$. The attitude $\underline{\boldsymbol{\Phi}}^\mathrm{T} = \begin{bmatrix} \Phi & \Theta & \Psi \end{bmatrix}$ is given in Euler angles describing bank, pitch, and heading angles.

In the sequel, we will refer to the piecewise polynomial equations of motion of [20] as the *prediction model*; and to the high-fidelity simulation [21] as the *simulation model*.

*Partly supported by ONERA – The French Aerospace Lab. The third author acknowledges support of the National Science Foundation Grant 1931738.

[1]TC, DL, and IK are with the Faculty of Aerospace Engineering, University of Michigan, Ann Arbor, Michigan 48109, USA, {tcunis,dliaomcp,ilya}@umich.edu.

[2]LB is with Rutgers, The State University of New Jersey, Piscataway, NJ 08854, USA, laurent.burlion@rutgers.edu.

II. Problem Setting

In this paper, we consider recovery approaches for the unthrottled aircraft (i.e., without thrust), in agreement with the FAA procedures [28]. The GTM represents a 5.5 % down-scaled, common passenger aircraft with an open-source high-fidelity simulation model implemented in Simulink that combines standard Newtonian equations of motion with extensive look-up tables for the static and dynamic aerodynamic coefficients based on wind-tunnel measurements and flight-test data. The state of the simulation consists of velocity, body rates, attitude, and position (the latter not considered here); inputs include surface deflection commands and engine throttle.

In the simulation model, the surface actuators are represented by first-order linear dynamics with restricted range and rate of response. Their dynamics are modelled as first order filers and can be written as

$$\dot{\delta}(t) = 2\pi f\,(\delta_{\mathrm{cmd}} - \delta(t)) \tag{1}$$

with $f = 5\,\mathrm{Hz}$ for $\delta \in \{\xi, \eta, \zeta\}$. Deflections are limited to $\xi \in \mathcal{X}_\xi = [-20°; 20°]$, $\eta \in \mathcal{X}_\eta = [-30°; 20°]$, and $\zeta \in \mathcal{X}_\zeta = [-30°; 30°]$. The actuator speed is limited to $\dot{\delta}_{\max} = 300\,°/\mathrm{s}$ for all surfaces.

In this paper, we consider recovery from steep spiral and period-one oscillatory spin upset conditions. Spiral and spin both are three-dimensional rotary motions, that is, they involve revolutions around more than one of the aircraft body axes. Hence, recovery requires coordinated effort of multiple, independent control inputs. Fig. 1 illustrates these flight conditions.* Here, the steep spiral mode is entered for an elevator deflection of $\eta = -30°$ and neutral rudder; the oscillatory spin mode is entered for elevator and rudder deflections of $\eta = -24°$ and $\zeta = -10°$, respectively.† Unlike oscillatory spin, the spiral motion is characterized by constant (non-zero) body rates; only the heading changes as the result of the steep spiral. Therefore, the spiral is technically a trim condition of aircraft flight. The oscillatory spin, in contrast, is in fact a periodic motion involving all three airspeed and aerodynamic angles, body rates, and attitude.

III. Controller Design

Our objective is to define a nonlinear MPC formulation that allows the aircraft to recover from an upset condition to an unthrottled, normal flight trim condition with low descent speed; specifically, we consider the following nominal, gliding trim condition for the subsequent

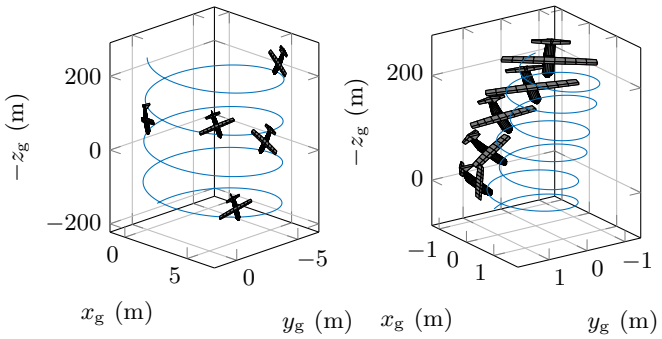

(a) Steep spiral. (b) Oscillatory spin.

Fig. 1: Spiral and oscillatory spin modes of the GTM (aircraft to scale).

simulation:

$$\begin{aligned} V_f &= 35.9\,\mathrm{m/s}, & \alpha_f &= 6.42°, & \beta_f &= 0°, \\ \boldsymbol{\omega}_f &= 0\,°/\mathrm{s}, & \Phi_f &= -0.037°, & \Theta_f &= 0.238°, \\ \xi_f &= -0.893°, & \eta_f &= -1.71°, & \zeta_f &< 0.005°, \end{aligned}$$

and $\dot{\Psi}_f = 0\,°/\mathrm{s}$. We use a discrete-time nonlinear prediction model of the following form

$$\mathbf{x}_{8\mathrm{e}}^{+} = \mathbf{x}_{8\mathrm{e}} + \tau\,\mathbf{f}_{8\mathrm{e}}(\mathbf{x}_{8\mathrm{e}}, \mathbf{x}_\delta)\,, \tag{2a}$$

$$\mathbf{x}_\delta^{+} = \mathbf{x}_\delta + \tau\,\mathbf{u}_\delta, \tag{2b}$$

where $\mathbf{f}_{8\mathrm{e}} : \mathbb{R}^8 \times \mathbb{R}^3$ are the continuous time equations of motion and the state and input vectors are

$$\mathbf{x}_{8\mathrm{e}}^T = \left[\begin{array}{ccc|ccc|cc} u & v & w & p & q & r & \Phi & \Theta \end{array}\right] \in \mathbb{R}^8, \tag{3a}$$

$$\mathbf{x}_\delta^T = \begin{bmatrix} \xi & \eta & \zeta \end{bmatrix} \in \mathcal{X}_\xi \times \mathcal{X}_\eta \times \mathcal{X}_\zeta = \mathcal{X}_\delta, \tag{3b}$$

$$\mathbf{u}_\delta^T = \begin{bmatrix} \dot{\xi} & \dot{\eta} & \dot{\zeta} \end{bmatrix} \in \mathcal{U}_\delta. \tag{3c}$$

The equations of motions $\mathbf{f}_{8\mathrm{e}}$ in (2) are the usual rigid body flight dynamics, viz.

$$\begin{aligned} m\dot{\mathbf{V}}_{\mathrm{A}} &= \mathbf{R}^{\mathrm{A}}(V_{\mathrm{A}}, \alpha, \beta, \xi, \eta, \zeta, \boldsymbol{\omega}) + \mathbf{R}^{\mathrm{G}} + m\boldsymbol{\omega} \times \mathbf{V}_{\mathrm{A}} \\ \mathrm{I}\dot{\boldsymbol{\omega}} &= \mathbf{Q}^{\mathrm{A}}(V_{\mathrm{A}}, \alpha, \beta, \xi, \eta, \zeta, \boldsymbol{\omega}) + \mathbf{Q}^{\mathrm{cg}} + \boldsymbol{\omega} \times \mathrm{I}\boldsymbol{\omega} \\ \dot{\underline{\boldsymbol{\Phi}}} &= \mathrm{M}_\omega(\underline{\boldsymbol{\Phi}})\,\boldsymbol{\omega} \end{aligned}$$

with vehicle mass m, matrix of inertia I, and Euler angle kinematic matrix M_ω. The weight force vector is denoted by $\mathbf{R}^{\mathrm{G}}$, the aerodynamic forces and moments by $\mathbf{R}^{\mathrm{A}}$ and $\mathbf{Q}^{\mathrm{A}}$, respectively, and $\mathbf{Q}^{\mathrm{cg}}$ are additional torques induced by displacement of the centre of gravity.

The aerodynamic forces $\mathbf{R}^{\mathrm{A}}$ and moments $\mathbf{Q}^{\mathrm{A}}$ are modelled using aerodynamic coefficients defined as piecewise polynomial functions around a near-stall switching point α_0. Exemplarily, the piecewise fit of the force coefficient along the body x-axis over the angle of attack can be found in Figure 2. A detailed description of the full model is available in [29, Eqs. (2.3)–(2.5), (2.7)–(2.9), (2.20) and Appendix B.1] as well as in [20].

The equation (2b) is a simplified discrete-time implementation of the actuator dynamics of (1) as integrator. We refer to (2) as the piecewise polynomial model. For

*In the figure, the aircraft drawing is roughly to scale and its orientation represents the aircraft attitude. The aircraft are depicted first at $t = 1.495\,\mathrm{s}$ and subsequently with a period of $\Delta t = 1.75\,\mathrm{s}$.

†The present GTM simulation appears to be robust with respect to spin; without a significant rudder deflection or exogenous inputs, the aircraft spin will eventually steady into a spiral (see [16] for a discussion of the effects of rudder onto spiral and spin modes).

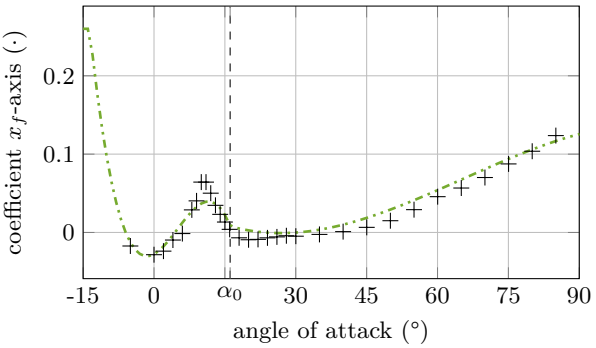

Fig. 2: Piecewise C_X-coefficient as function of α.

the model, we use the (desired) actuator rates $\dot{\xi}, \dot{\eta}, \dot{\zeta}$ as inputs and choose a sampling period $\tau = 50\,\text{ms}$. The set of admissible state-input pairs is then $\mathcal{Z} = \mathbb{R}^8 \times \mathcal{X}_\delta \times \mathcal{U}_\delta$. Note that, although we have not directly incorporated the actuator dynamics of (1) into the prediction model, we limit the actuator rates such that $|2\pi f\,(\delta^+ - \delta(t))| \leq \dot{\delta}_{\max}$ for all $t \in [0;\tau)$; i.e.,

$$\mathcal{U}_\delta = \left[-\frac{\dot{\delta}_{\max}}{2\pi f \tau}; +\frac{\dot{\delta}_{\max}}{2\pi f \tau} \right]^3 .$$

We also normalize the states and inputs to improve the scaling of the prediction model. After scaling of states and inputs, we denote the combined state vector by $\tilde{\mathbf{x}}^{\mathrm{T}} = \left[\begin{array}{c:c} \mathbf{D}_{\mathbf{x}_{8e}}^{-1}\mathbf{x}_{8e} & \mathbf{D}_{\mathbf{x}_\delta}^{-1}\mathbf{x}_\delta \end{array} \right]$, the scaled input vector by $\tilde{\mathbf{u}} = \mathbf{D}_{\mathbf{u}_\delta}^{-1}\mathbf{u}_\delta$, the discrete system by $\tilde{\mathbf{x}}^+ = \mathbf{f}^+(\tilde{\mathbf{x}}, \tilde{\mathbf{u}})$, and the steady-state control inputs are $\tilde{\mathbf{u}}_f = 0$. The scaling matrices are given in the appendix.

A. Optimal Control Problem Formulation

The MPC feedback law $\boldsymbol{\mu}_N(\cdot)$ is based on solving the following finite-horizon optimal control problem (OCP)

$$\min_{\tilde{\mathbf{x}}_{(\cdot)}, \tilde{\mathbf{u}}_{(\cdot)}} \sum_{k=1}^{N-1} \ell(\tilde{\mathbf{x}}_k, \tilde{\mathbf{u}}_k) \tag{4a}$$

$$\text{s.t. } \tilde{\mathbf{x}}_{k+1} = \mathbf{f}^+(\tilde{\mathbf{x}}_k, \tilde{\mathbf{u}}_k), \quad k \in [1;N) \tag{4b}$$

$$\tilde{\mathbf{x}}_k \in \mathbb{R}^8 \times \tilde{\mathcal{X}}_\delta, \quad k \in [1;N) \tag{4c}$$

$$\tilde{\mathbf{u}}_k \in \tilde{\mathcal{U}}_\delta, \quad k \in [1;N) \tag{4d}$$

$$\tilde{\mathbf{x}}_N = \tilde{\mathbf{x}}_f, \tag{4e}$$

where $\mathbf{x}(t) = \mathbf{D}_{\mathbf{x}}\tilde{\mathbf{x}}_1$ is the measured state at time t, $N = 120$ is the prediction horizon (equal to 6 s), tracking stage cost is given by

$$\ell(\tilde{\mathbf{x}}, \tilde{\mathbf{u}}) = \frac{1}{2}\left\|\tilde{\mathbf{x}} - \tilde{\mathbf{x}}_f\right\|_{\tilde{\mathrm{E}}}^2 + \frac{1}{2}\left\|\tilde{\mathbf{u}}\right\|_{\tilde{\mathrm{F}}}^2, \tag{5}$$

with $\|\mathbf{x}\|_{\mathrm{E}}^2 = \mathbf{x}^T\mathrm{E}\mathbf{x}$, $\tilde{\mathrm{E}} = \mathbb{I}_{11}$, and $\tilde{\mathrm{F}} = \mathbb{I}_3/100$, and $\tilde{\mathbf{x}}_f$ is the nominal gliding trim condition defined above given in scaled variables. The MPC feedback is then given by $\boldsymbol{\mu}_N(\mathbf{x}(t)) = \mathbf{D}_{\mathbf{u}_\delta}\hat{\mathbf{u}}_1$ if $\hat{\mathbf{u}}$ solves (4).

Weights were picked based on numerical experience and the horizon length was chosen to be long enough to capture the entire recovery manoeuvre. We use a terminal state constraint to guarantee nominal closed-loop stability. In the future, we plan to switch to a less stringent pair of terminal penalty and terminal region constraint, computed using sum-of-squares programming techniques, to enlarge the closed-loop region of attraction.

As the tracking cost function in (5) is positive-definite, asymptotic stability of the nominal closed-loop dynamics follows from [29, Theorem II.4] under the assumption of weak controllability. Note that in the presence of model mismatch offset-free tracking is not guaranteed. In an upset recovery scenario, convergence to an slightly different but stable trim condition is acceptable closed-loop behaviour. Another option would be switching to a nominal flight controller (with integral action) once the aircraft has recovered [24].

B. Implementation Details

We solve the OCP in Eq. (4) using the nonlinear interior-point solver `Ipopt` [30]. The functions necessary to solve the problem, such as the objective function as well as its gradient vector and Hessian matrix, were generated using CasADI [31] and compiled into MATLAB's binary `mex` file format to increase evaluation speed. The computed optimal trajectories for a time t_0 are subsequently used as initial guess for $\mathbf{x}(t_0 + \tau)$.

We elected to use a multiple-shooting (where the state and control inputs are considered optimization variables) formulation for the OCP (4) rather than a single-shooting approach (where only control inputs are considered optimization variables). The computational complexity of multiple-shooting methods scale linearly with N while single-shooting methods scale like N^3, as the prediction horizon is relatively long ($N = 120$), the multiple shooting approach is better suited to our problem.

IV. High-fidelity Simulation Results

In this section we present simulation results where the MPC controller, which uses the piecewise polynomial prediction model, is run in closed-loop with the high-fidelity GTM. The GTM is implemented in Simulink and uses a fixed-step `ode3` solver operating at a frequency of 200 Hz, 10 times faster than the discrete prediction model ($\tau^{-1} = 20\,\text{Hz}$). The OCP (4) is solved at the lower frequency of 20 Hz and the control input is subsequently held constant between sampling instances. The optimal control inputs, the actuator rates returned by $\boldsymbol{\mu}_N(\cdot)$, are converted into the deflection commands as

$$\delta_{\mathrm{cmd}}(t) = \delta(t_0) + \tau\,\dot{\delta}_{\boldsymbol{\mu}} \tag{6}$$

for all $t \in [t_0; t_0 + \tau)$, where $\dot{\delta}_{\boldsymbol{\mu}}$ is the MPC feedback for $\mathbf{x}(t_0)$. As the time constant of (1) is smaller than τ, the actuators will not reach the commanded deflection within one period of the MPC feedback. This results in mismatch between the simulation and prediction models.

Furthermore, the simulation computes the dynamic coefficients using the hybrid Kalviste method [32], whereas the piecewise polynomial model directly evaluates the aerodynamic coefficients for the body rates. The MPC feedback is evaluated for the first time at $t = \tau$. We assume full state feedback is available throughout.

A. *Recovery from steep spiral*

Fig. 3 details the aircraft's flight path and attitude during recovery. Note that the depiction of the aircraft is enlarged here for clarity. We observe that, due to a quick recovery of the bank angle, the the aircraft is recovered from its spiral motion without further change of the heading despite the initial rotatory flight condition.

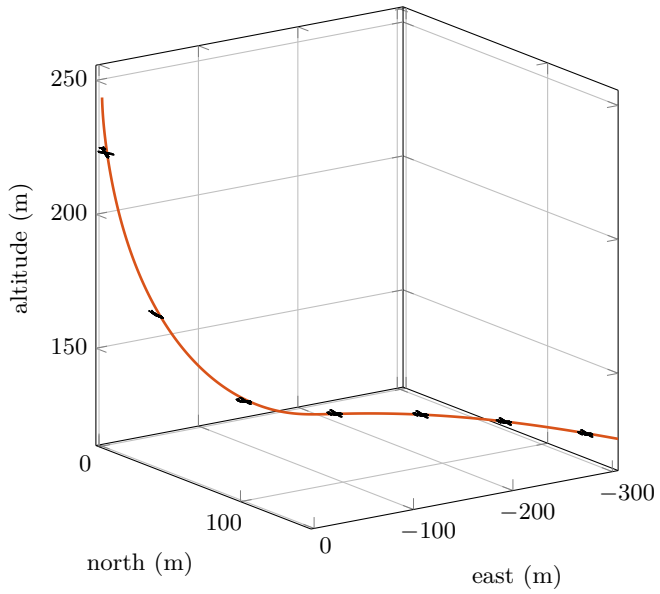

Fig. 3: Flight path of steep spiral recovery (aircraft *not* to scale).

Fig. 4 shows the aircraft states during simulated recovery from the steep spiral upset condition. Figure 4 also shows the state values predicted for the next step, i.e., $\hat{\mathbf{x}}(t) = \hat{\mathbf{x}}_1$ for $t \in [t_0; t_0 + \tau)$ if $\hat{\mathbf{x}}_{(\cdot)}$ is the optimal trajectory for $\mathbf{x}(t_0)$. Here, commanded and one-step ahead predicted actuator deflections are equal despite the mismatch of modelled integrator dynamics and simulated first-order damping. The bank angle is recovered first with an angle of attack of about 15°. After 4 s the aircraft is levelled and the longitudinal flight condition is restored by reducing angle of attack and air speed.

B. *Recovery from oscillatory spin*

Fig. 5 shows the time history of the simulated oscillatory spin recovery.[‡] During early restoration of the bank

[‡]Note that due to the delayed engagement of the MPC feedback only after one period τ and the fact that the oscillatory spin constitutes a periodic motion, the first state of the simulated MPC recovery has been slightly evolved compared to the initial condition of the aircraft simulation, which has coincided with the initial condition for the nominal MPC recovery.

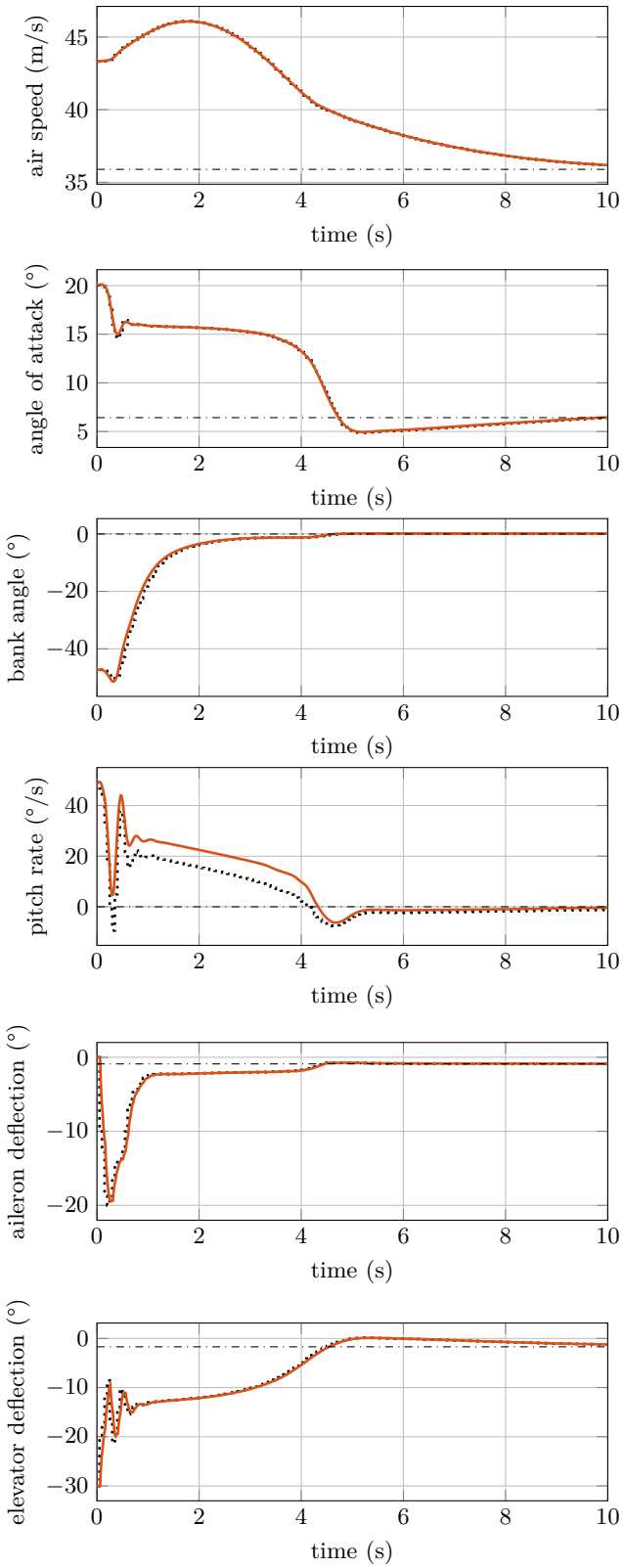

Fig. 4: Simulated recovery from steep spiral upset. Simulation in solid (——), one-step prediction dotted (·····).

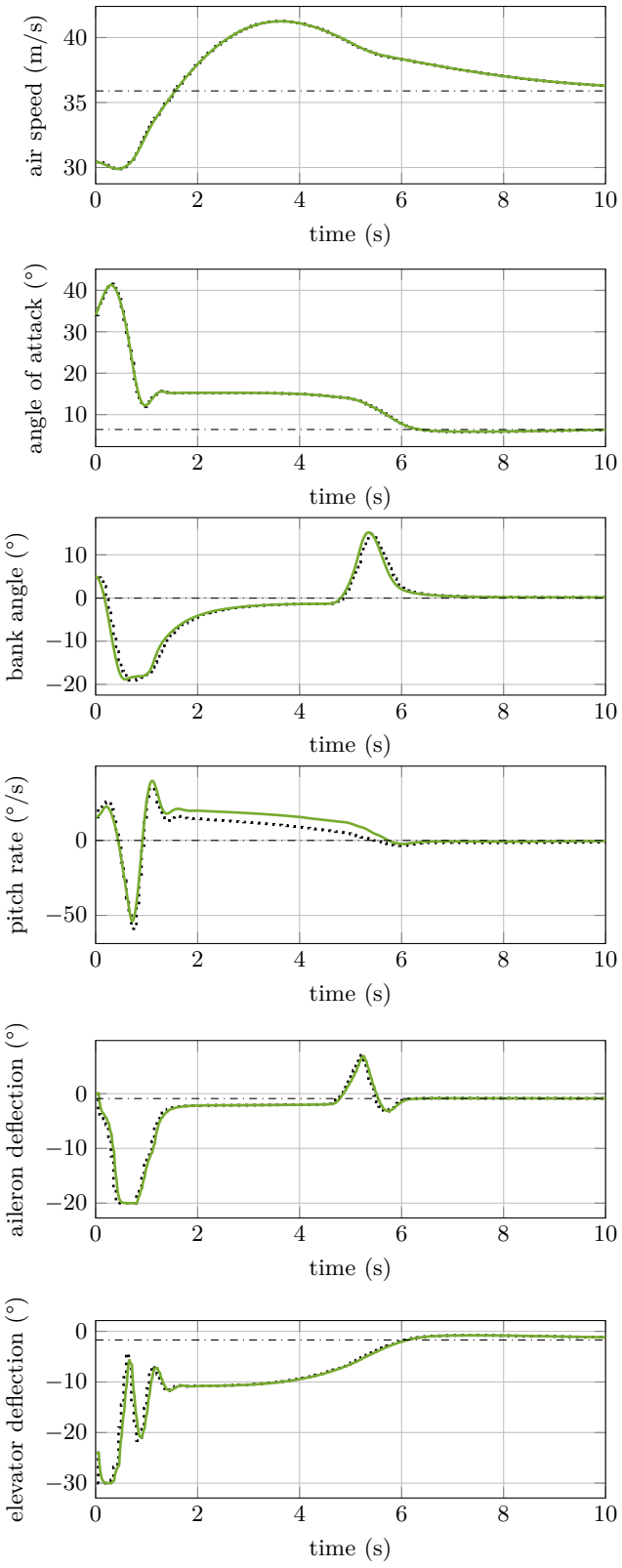

Fig. 5: Simulated recovery from oscillatory spin. Simulation in solid (——), one-step prediction dotted (·····).

angle, the ailerons operate at the lower limit for almost 400 ms but are moved to a near-neutral position soon after. Right before the aircraft's angle of attack is fully restored, and after bank angle and aileron deflections have been close to the trim condition for some time, we observe a spike in the lateral motion initiated by a sharp deflections of ailerons and rudder. It is only afterwards that, together with the angle of attack, the bank angle is fully restored.

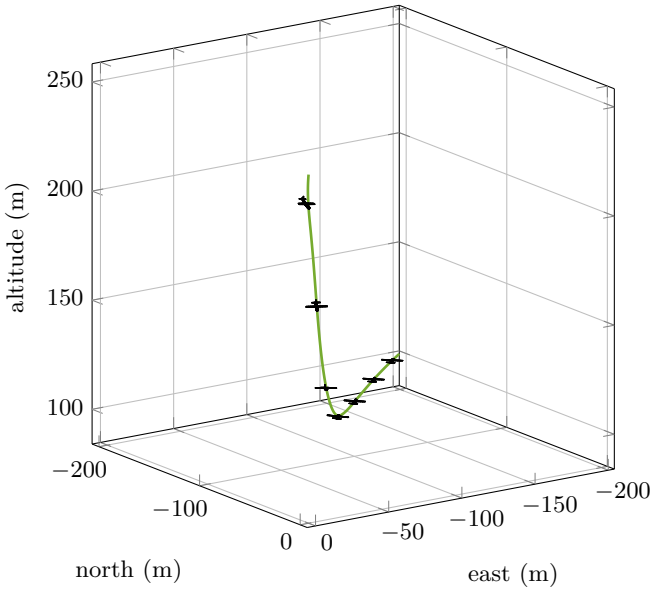

Fig. 6: Flight path of oscillatory spin recovery (aircraft *not* to scale).

The flight path (Fig. 6) further reveals a quick recovery of the lateral spin motion. Note that the recovery time during the high-fidelity simulations is longer than the prediction horizon, despite the terminal state constraint being successfully enforced. Due to the receding horizon nature of the MPC formulation convergence is asymptotic despite finite time convergence being possible. Achieving minimum or finite-time convergence in MPC requires specific formulations such as [33, 34].

C. Discussion

Overall, the piecewise polynomial prediction model provides reasonably accurate predictions of the one-step ahead future aircraft states during recovery both from steep spiral and oscillatory spin upsets. However, during both manoeuvres, we observe a stark disparity between the predicted and actual pitch rates while the bank angle is recovered. Here, the angle of attack and the elevator deflection are both roughly constant an equal to $\alpha = 15°$ and $\eta = -10°$, respectively. Comparison of look-up table data and polynomial model for the pitch-moment coefficient C_m, in Fig. 7, reveals a highly inaccurate model for these conditions. It is worth noting that polynomials of higher degrees than the used 3rd-order polynomials of [20] could improve model accuracy.

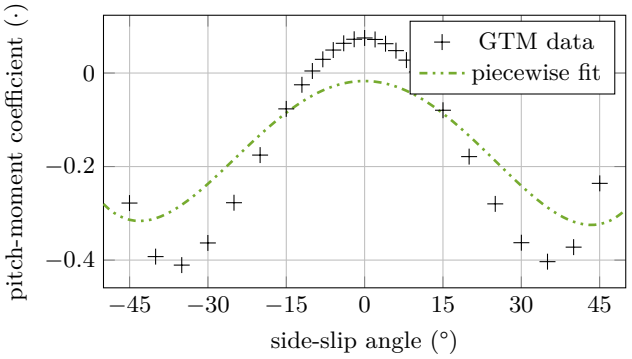

Fig. 7: Piecewise polynomial C_m model over β for $\alpha = 15°$, $\eta = -10°$.

It might be interesting to further compare the optimizing MPC recovery strategies to switching control approaches such as presented in [10] or [11]. In fact, the MPC recovery reveals some sequential elements for the recovery of angle of attack and side-slip, reduction of roll and yaw rate, as well as bank angle restoration.

First, angle of attack and side-slip[§] are reduced – yet not recovered – and the body rates are regulated. Only after restoration of the bank angle, the angle of attack and side-slip are fully recovered, too. In that, the MPC recovery contrasts the approach of [10] which emphasised the recovery of aerodynamic angles over attitude. The work of [11], on the other hand, focused on the regulation of body rates first before recovering all three angle of attack, side-slip angle, and bank angle. As in the switching approaches, the MPC recovery restores air speed last.

In [29, Chapter 8], the closed-loop behaviour of the nominal model has been discussed for first insights into model-predictive upset recovery strategies. We observe that for both spiral and oscillatory spin the simulated recovery on the high-fidelity model is faster than on the nominal model while remaining qualitatively similar. Despite being incidental, the lower recovery time of the simulation compared to the nominal model indicates that the aircraft behaviour is relatively benign (in terms of spiral and spin upsets). Indeed, previous analyses have indicated that reduction of the angle of attack suffices for spiral recovery [16] and neutral position of the rudder leads to the relaxation of oscillatory spin into a spiral motion.

D. Computational Footprint

During our high-fidelity simulations it took, on average, below 1 s to compute the the optimal control action (Intel Core i7, 3 GHz, 16 GB): Only the first OCP, for which no proper initial guess exists, required 13.3 s and 28.4 s, respectively; once an initial guess was available, the computation took on average 0.707 s (worst-case 1.70 s) and 0.849 s (worst-case 2.12 s).

[§]The side-slip angle is not shown in Figs. 4 and 5.

Our current implementation is too slow for real-time deployment but is sufficient to demonstrate that MPC feedback laws are capable of recovering the aircraft, despite model mismatch and noise. Further reduction of the computation times is imperative for future work integrating model-predictive recovery strategies into real aircraft systems. As a result, the next step is to achieve real-time feasibility by exploiting efficient implementations or real-time methods such as [35, 36]. Considering recovery of a full-sized transport aircraft, the use of a moderately-sized desktop computer and precomputing recovery trajectories for solver warm-start are reasonable assumptions.

V. Concluding Remarks

This paper presented a nonlinear MPC based 6dof upset recovery strategy and demonstrated its effectiveness through closed-loop simulations using the high-fidelity GTM model. We have demonstrated, through successful simulated recoveries from spiral and spin upsets, that the piecewise prediction model is sufficiently accurate, and that the MPC approach is sufficiently robust against uncertainties, to allow the MPC controller to recover the aircraft despite the mismatch between the prediction and the actual dynamics (as reflected in the high-fidelity simulation). Future work includes investigating the robustness properties of the proposed MPC controller, additional development to reduce the computational footprint, and experiments on small drones.

Appendix

The singular non-differentiable point of the piecewise polynomial aerodynamic models (namely, at α_0) were again smoothened by the Heaviside step function $\mathcal{H}(\alpha) = \frac{1}{1+e^{-2\alpha/\nu}}$ and the parameter ν has been reduced from $\frac{\pi}{36}$ for the first iteration down to $\frac{\pi}{576}$ for the fifth and all following iterations. States and inputs of the discrete nonlinear dynamics are scaled by

$$\begin{aligned}\mathbf{D}_{\mathbf{x}_{8\mathrm{e}}} &= \mathrm{diag}(40\,\mathrm{m/s}, 25\,\mathrm{m/s}, 35\,\mathrm{m/s}, 50\,°/\mathrm{s},\\ &\qquad 100\,°/\mathrm{s}, 50\,°/\mathrm{s}, 30°, 45°)\,,\\ \mathbf{D}_{\mathbf{x}_\delta} &= \mathrm{diag}(15°, 20°, 25°)\,,\\ \mathbf{D}_{\mathbf{u}_\delta} &= \mathrm{diag}(150\,°/\mathrm{s}, 150\,°/\mathrm{s}, 150\,°/\mathrm{s})\,.\end{aligned}$$

References

[1] *Loss of Control In-Flight Accident Analysis Report, 2010–2014*. Montreal, CA: International Air Transport Association, 2015.

[2] M. H. Smaili, J. Breeman, T. J. J. Lombaerts, J. A. Mulder, Q. P. Chu, and O. Stroosma, "Intelligent Flight Control Systems Evaluation for Loss-of-Control Recovery and Prevention," *Journal of Guidance, Control, and Dynamics*, vol. 40, no. 4, pp. 890–904, 2016.

[3] N. D. Richards, N. Gandhi, A. J. Bateman, D. H. Klyde, and A. K. Lampton, "Vehicle Upset Detection and Recovery for Onboard Guidance and Control," *Journal of Guidance, Control, and Dynamics*, vol. 40, no. 4, pp. 920–933, 2017.

[4] R. C. Allen, H. G. Kwatny, and G. Bajpai, "Safe Set Protection and Restoration for Unimpaired and Impaired Aircraft," in *AIAA Guidance, Navigation, and Control Conference*, Minneapolis, US-MN, 2012.

[5] B.-C. Chang, H. G. Kwatny, E. R. Ballouz, and D. C. Hartmann, "Aircraft Trim Recovery from Highly Nonlinear Upset Conditions," in *AIAA Guidance, Navigation, and Control Conference*, San Diego, US-CA, 2016.

[6] H. J. Tol, C. C. de Visser, L. G. Sun, E. van Kampen, and Q. P. Chu, "Multivariate Spline-Based Adaptive Control of High-Performance Aircraft with Aerodynamic Uncertainties," *Journal of Guidance, Control, and Dynamics*, vol. 39, no. 4, pp. 781–800, 2016.

[7] D. Kim, G. Oh, Y. Seo, and Y. Kim, "Reinforcement Learning-Based Optimal Flat Spin Recovery for Unmanned Aerial Vehicle," *Journal of Guidance, Control, and Dynamics*, vol. 40, no. 4, pp. 1076–1084, 2016.

[8] S. R. Schuet, T. J. J. Lombaerts, J. Kaneshige, K. H. Shish, and V. Stepanyan, "Stall Recovery Guidance Using Fast Model Predictive Control," in *AIAA Guidance, Navigation, and Control Conference*, Grapevine, US-TX, 2017.

[9] J. J. K. Engelbrecht and J. A. A. Engelbrecht, "Optimal attitude and flight vector recovery for large transport aircraft using sequential quadratic programming," in *2016 Pattern Recognition Association of South Africa and Robotics and Mechatronics International Conference*, Stellenbosch, SA, 2016.

[10] J. A. A. Engelbrecht, S. J. Pauck, and I. K. Peddle, "A Multimode Upset Recovery Flight Control System for Large Transport Aircraft," in *AIAA Guidance, Navigation, and Control Conference*, Boston, US-MA, aug 2013.

[11] A. Yildiz, M. U. Akcal, B. Hostas, and N. K. Ure, "Switching Control Architecture with Parametric Optimization for Aircraft Upset Recovery," *Journal of Guidance, Control, and Dynamics*, 2019.

[12] P. F. A. Di Donato, S. Balachandran, K. McDonough, E. Atkins, and I. Kolmanovsky, "Envelope-aware Flight Management for Loss of Control Prevention given Rudder Jam," *Journal of Guidance, Control, and Dynamics*, vol. 40, pp. 1027–1041, 2017.

[13] K. McDonough and I. Kolmanovsky, "Fast Computable Recoverable Sets and Their Use for Aircraft Loss-of-Control Handling," *Journal of Guidance, Control, and Dynamics*, vol. 40, no. 4, pp. 934–947, 2017.

[14] J. V. Foster, K. Cunningham, C. M. Fremaux, G. H. Shah, and E. C. Stewart, "Dynamics Modeling and Simulation of Large Transport Airplanes in Upset Conditions," in *AIAA Guidance, Navigation, and Control Conference and Exhibit*, San Francisco, US-CA, aug 2005.

[15] T. L. Jordan, J. V. Foster, R. M. Bailey, and C. M. Belcastro, "AirSTAR: A UAV Platform for Flight Dynamics and Control System Testing," in *AIAA Aerodynamics Measurement Technology and Ground Testing Conference*, San Francisco, US-CA, 2006.

[16] S. J. Gill, M. H. Lowenberg, S. A. Neild, B. Krauskopf, G. Puyou, and E. Coetzee, "Upset Dynamics of an Airliner Model: A Nonlinear Bifurcation Analysis," *Journal of Aircraft*, vol. 50, no. 6, pp. 1832–1842, aug 2013.

[17] L. Grüne and J. Pannek, *Nonlinear Model Predictive Control: Theory and Algorithms*, 2nd ed. Basel, CH: Springer, 2017.

[18] J. B. Rawlings, D. Q. Mayne, and M. Diehl, *Model Predictive Control: Theory, Computation, and Design*, 2nd ed. Santa Barbara, US-CA: Nob Hill, 2017.

[19] T. Cunis, L. Burlion, and J.-P. Condomines, "Piecewise Polynomial Modeling for Control and Analysis of Aircraft Dynamics beyond Stall," *Journal of Guidance, Control, and Dynamics*, vol. 42, no. 4, pp. 949–957, 2019.

[20] ——, "Piecewise Polynomial Model of the Aerodynamic Coefficients of the Generic Transport Model and its Equations of Motion," ONERA – The French Aerospace Lab; French Civil Aviation School, Toulouse, FR, Tech. Rep. `hal-01808649`, version 3, 2018. [Online]. Available: https://archives-ouvertes.fr/hal-01808649v3

[21] "Flight Dynamics Simulation of a Generic Transport Model," Hampton, US-VA, 2016. [Online]. Available: https://software.nasa.gov/software/LAR-17625-1

[22] U. Eren, A. Prach, B. B. Koçer, S. V. Raković, E. Kayacan, and B. Açıkmeşe, "Model Predictive Control in Aerospace Systems: Current State and Opportunities," *Journal of Guidance, Control, and Dynamics*, vol. 40, no. 7, pp. 1541–1566, 2017.

[23] L. Ferranti, Y. Wan, and T. Keviczky, "Fault-tolerant reference generation for model predictive control with active diagnosis of elevator jamming faults," *International Journal of Robust and Nonlinear Control*, 2018.

[24] T. Cunis, D. Liao-McPherson, J.-P. Condomines, L. Burlion, and I. Kolmanovsky, "Economic Model-Predictive Control Strategies for Aircraft Deep-stall Recovery with Stability Guarantees," in *58th IEEE Conference on Decision and Control*, Nice, FR, 2019, pp. 157–162.

[25] G. B. Gratton, R. I. Hoff, A. Rahman, C. Harbour, S. Williams, and M. Bromfield, "Evaluating a set of stall recovery actions for single engine light aeroplanes," *The Aeronautical Journal*, vol. 118, no. 1203, pp. 461–484, 2014.

[26] R. A. Bunge and I. M. Kroo, "Automatic Spin Recovery with Minimal Altitude Loss," in *2018 AIAA Guidance, Navigation, and Control Conference*, Kissimmee, US-FL, 2018.

[27] *Flight dynamics – Concepts, quantities and symbols – Part 3: Derivatives of forces, moments and their coefficients*, 2nd ed. Genève, CH: International Organization for Standarization, 1989.

[28] "Airplane Flying Handbook," Flight Standards Service, Washington, US-DC, FAA handbook FAA-H-8083-3B, 2016.

[29] T. Cunis, "Modeling, Analysis, and Control for Upset Recovery: From system theory to unmanned aircraft flight," Doctoral thesis, ISAE-Supaéro, Université de Toulouse, Toulouse, FR, 2019. [Online]. Available: https://tel.archives-ouvertes.fr/tel-02555908

[30] A. Wächter and L. T. Biegler, "On the implementation of an interior-point filter line-search algorithm for large-scale nonlinear programming," *Mathematical Programming, Series A*, vol. 106, pp. 25–57, 2006.

[31] J. A. E. Andersson, J. Gillis, G. Horn, J. B. Rawlings, and M. Diehl, "CasADi – A software framework for nonlinear optimization and optimal control," *Mathematical Programming Computation*, vol. 11, pp. 1–36, 2019.

[32] A. M. Murch and J. V. Foster, "Recent NASA Research on Aerodynamic Modeling of Post-Stall and Spin Dynamics of Large Transport Airplanes," in *45th AIAA Aerospace Sciences Meeting and Exhibit*. Reno, US-NV: American Institute of Aeronautics and Astronautics, jan 2007.

[33] R. L. Sutherland, I. V. Kolmanovsky, A. R. Girard, F. A. Leve, and C. D. Petersen, "On closed-loop lyapunov stability with minimum-time mpc feedback laws for discrete-time systems," in *2019 IEEE 58th Conference on Decision and Control (CDC)*. IEEE, 2019, pp. 5231–5237.

[34] C. Rösmann, A. Makarow, and T. Bertram, "Stabilizing quasi-time-optimal nonlinear model predictive control with variable discretization," *arXiv preprint arXiv:2004.09561*, 2020.

[35] M. Diehl, R. Findeisen, F. Allgöwer, H. G. Bock, and J. P. Schlöder, "Nominal stability of real-time iteration scheme for nonlinear model predictive control," *IEE Proceedings – Control Theory and Applications*, vol. 152, no. 3, pp. 296–308, may 2005.

[36] D. Liao-McPherson, M. Nicotra, and I. Kolmanovsky, "Time-distributed optimization for real-time model predictive control: Stability, robustness, and constraint satisfaction," *Automatica*, vol. 117, p. 108973, 2020.